

# Experimental Information on the Mass Composition of Primary Cosmic Rays Using the KASCADE array

Tadeusz Wibig

*Experimental Physics Dept., University of Lodz, Pomorska 149/153, 90-236 Lodz, Poland*

---

## Abstract

A procedure is proposed to extract experimental information about the primary cosmic Ray composition from the data taken with the KASCADE setup.

---

## 1 Introduction

The data collected with the KASCADE detector setup (Ref. [1]) carry information first about the electromagnetic component of extensive air showers (EAS), sufficiently accurately to enable the reconstruction of the shower core position and the angle of incidence, and to determine the electron–photon density distribution (at least at larger distances from the center) for individual shower. For the analysis proposed in this note only the knowledge of the electron–photon density at a particular fixed distance  $r$  will be needed. The accuracy of its determination, dependent on shower size, core location and inclination of the shower, can be expected to be in the order of few percent.

For the muon component data will be measured for different energy thresholds of various muon detector devices of KASCADE. The array registers muons with energies above 100 MeV, while the muon multiwire proportional chamber installation below the iron–sampling calorimeter of the central detector has a muon detection threshold of 2 GeV. In addition there is a muon tracking hodoscope setup in a tunnel under installation with the threshold of 900 MeV. The different data sets may be analyzed separately, providing cross checks, or in a combined way, increasing the accuracy of the estimated muon distribution parameters. That accuracy is certainly worse than for the electron–photon component, first of all due to the lower densities of the muon component.

Nevertheless the uncertainty of the muon density at some intermediate distance from the core may be not larger than about 20%. In addition to the muon density at the fixed distance  $r$ , an additional parameter of the muon lateral distribution can be extracted and used for the analysis. Most promising appears the slope of that distribution ( defined by  $-\left(\frac{d \ln \rho_\mu}{d \ln r}\right)$  at the fixed radial distance  $r$  ). The accuracy of its determination is not a crucial for the proposed procedure of the data analysis.

## 2 Method

For the CR showers registered by the experiment the density correlation can be displayed in two-dimensional histogram in  $(\rho_\mu(r_0), \rho_e(r_0))$ , similar to the well-known  $(N_\mu, N_e)$  plot. From the experimental point of view the densities at a fixed distance can be much better defined so the experimental uncertainties concerning the  $N_\mu$  and  $N_e$  determination vanish.

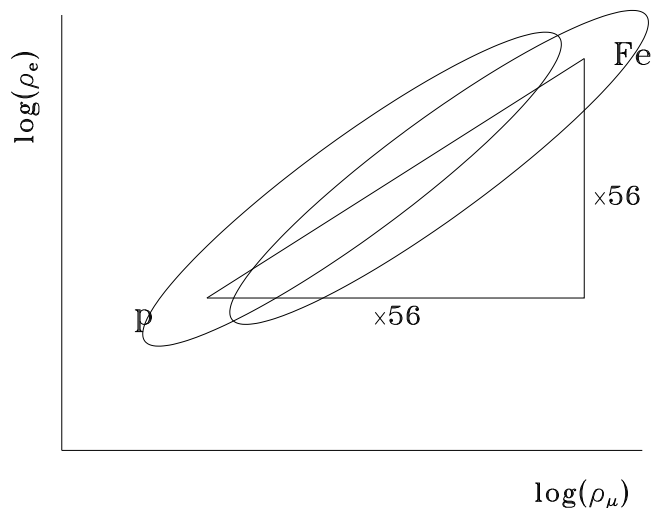


Fig. 1. Positions of the points representing individual showers initiated by the primary protons and iron nuclei in the two-dimensional plot  $\ln(\rho_\mu(r_0)) \times \ln(\rho_e(r_0))$ .

In the Fig.1 there are schematically presented points appearing in the  $(\rho_\mu(r_0), \rho_e(r_0))$  plot for proton and iron induced showers. The vector  $(56 \times, 56 \times)$  gives the connection between the two groups and it is a consequence of the compositeness of the iron nucleus and it is very hard to change that factor much using any sophisticated interaction model. The simple superposition model leads to the

exact 56 value. The more realistic calculations shows that the mean values of shower characteristics are in surprising good agreement with the superposition assumption (Ref. [2]) only fluctuations are larger then expected ( $1 / \sqrt{A\sigma_p}$ ). This is quite obvious because subshowers in the composite nucleus cascade are not independent. Divergences in the mean values are mainly due to the effects of differences in interaction cross-sections used and the details in nucleus-nucleus interaction treatment.

If for each  $(\rho_\mu(r_0), \rho_e(r_0))$  bin the average value of the  $\mu$  distribution slope parameter will be given that for the proton showers the clear dependence is expected.

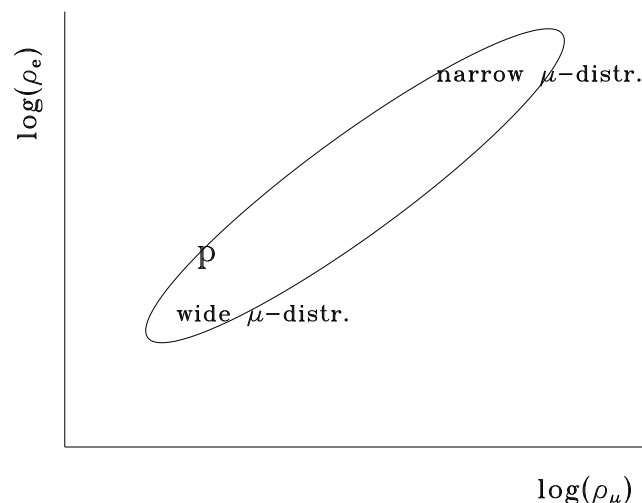


Fig. 2. The expected change in the  $\mu$  distribution slope parameter for the proton induced showers of different electron and muon sizes.

For the smaller showers muons has to be distributed wider than for the larger ones.

That situation is presented in details in the Fig.8. The same dependence is of course expected for any kind of primary particle (Fig. 9) because it is a simple result of the geometry of the shower development. It is again rather hard to think about the shower model without such a behaviour. For the more energetic primary particle extensive air shower has to developed deeper in the atmosphere so there must be an increase of the number of muons observed on the ground generated closer to the observation level. If no unexpected change of the interaction picture is assumed than all that muons has to be distributed closer to the shower axis simply because of that they have no time to wander

broaden.

In the Fig. 3 the situation for proton and iron initiated showers is shown.

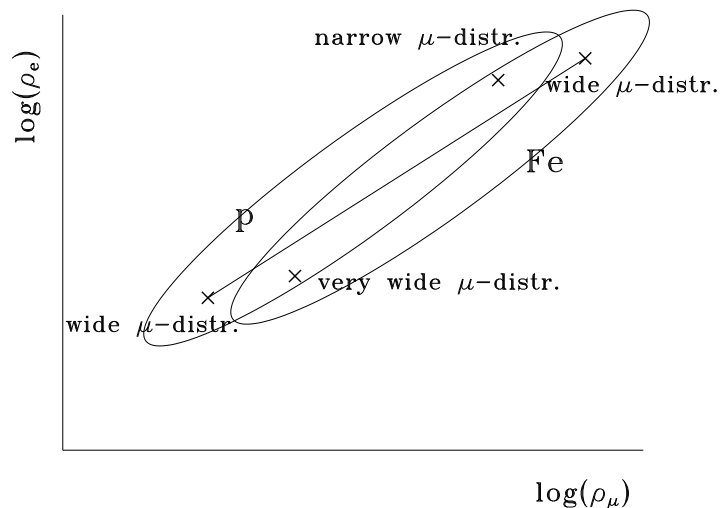


Fig. 3. The expected change in the  $\mu$  distribution slope parameter for the proton and iron induced showers.

If we shift the "wide proton shower points" by the vector  $(56\times, 56\times)$  we obtain the points for iron showers with approximately the same energy per nucleon. The slope of the  $\mu$  lateral distribution has to be approximately the same. The word "approximately" in the last sentence has the different meaning than the same word in the previous one. While the first is, as discussed above, related to the applicability of the superposition model for the mean value of the electron and muon densities in the shower, the second is much sensitive to the shower development fluctuations.

However the calculation shows (see Figs. 8–13, 15 and 16) that the effect is so big that the spread due to the fluctuations of the proton shower development for the fixed primary energy is not able to diminish it. This is the main point of the analysis proposed.

For the primary spectrum with the one component only (e.g. protons) the slope for fixed value of  $\rho_\mu(r_0)$  (or  $\rho_e$ ) should not change very much but if we assume that there is an important fraction of other (heavier) nuclei in the primary CR mass spectrum the  $\mu$  slope has to change from the one given in Fig. 4.:

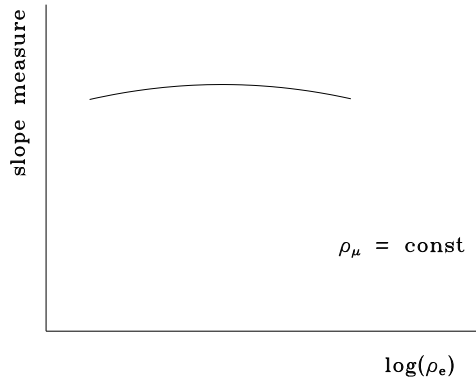


Fig. 4. The slope of the  $\mu$  distribution measure of the proton induced showers as a function of the muon density at the fixed distance from the shower core for the showers with the given electron density at some fixed distance.

to the one presented below in Fig. 5:

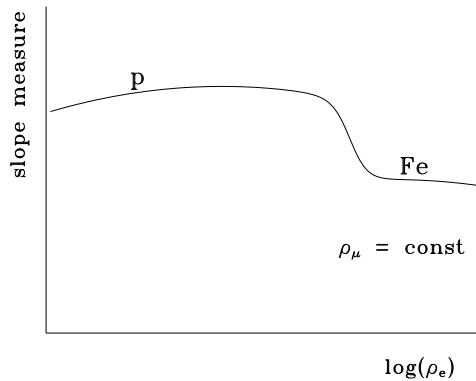


Fig. 5. The slope of the  $\mu$  distribution measure of the proton and iron in the primary CR spectrum as a function of the muon density at the fixed distance from the shower core for the showers with the given electron density at some fixed distance.

Details can be seen in Figs. 10 and 11.

In the real case the primary CR mass spectrum is much complex than protons and iron nuclei only. In that case there are some points on  $(\rho_\mu(r_0), \rho_e(r_0))$  plot shifted from the pure proton picture also by the vectors  $(28\times, 28\times)$ ,

$(14\times, 14\times)$  and  $(4\times, 4\times)$  for Ne-S, C-O and He nuclei group respectively. This is shown schematically in Fig. 6.

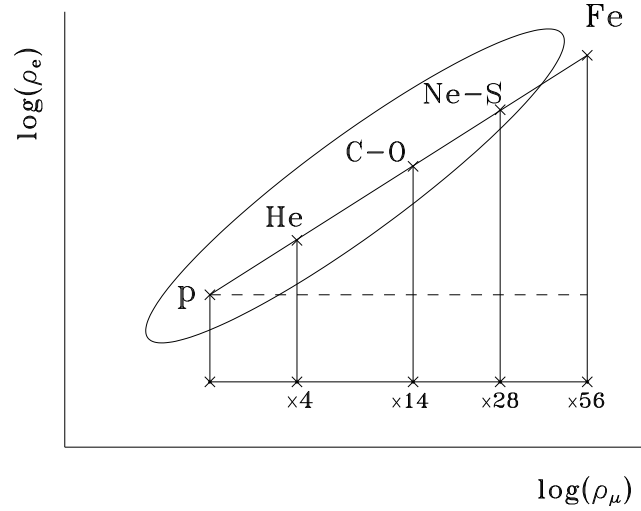


Fig. 6. Positions of the points representing individual showers initiated by the primary protons, He, C-O, Ne-S and Fe nuclei in the two-dimensional plot  $\ln(\rho_\mu(r_0)) \times \ln(\rho_e(r_0))$ .

The "realistic" view is given below.

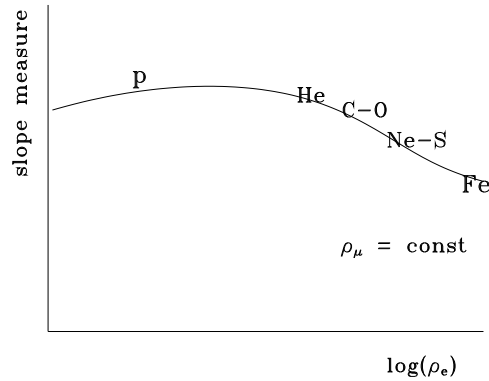


Fig. 7. The slope of the  $\mu$  distribution measure of the proton and iron in the primary CR spectrum as a function of the muon density at the fixed distance from the shower core for the showers with the given electron density at some fixed distance.

It makes the situation from Fig. 5 less clear, anyhow points to the left in the Fig. 6 have to give the  $\mu$ -slope of the proton showers (if there are protons at all in the primary CR spectrum) while points the most to the right will give the  $\mu$ -slope of the iron (again: if there is any). Only the detail shape of change from the left-side to the right-side value is related to the different nuclei abundances in primary CR.

Results of calculations are presented in Fig. 12. The mass spectrum used was the one measured recently by JACEE group (Ref. [3]) at about  $10^{14}$  eV per nucleus  $H : He : C - O : Ne - S : Fe \sim 24\% : 33\% : 16\% : 14\% : 13\%$ .

The statistics of showers shown is approximately the same as for about one week of the KASCADE data collecting. The measure of the  $\mu$ -slope used is  $\left(-\frac{d\ln\rho_\mu}{d\ln r}\right)$  at the distance from the shower core  $r_0 = 50m$ .

In the Fig. 8 the results on the slope measure for pure proton spectrum is given. The comparison of this results with the one in Fig. 9 for pure iron spectrum shows that the slope measure differs significantly (as it was expected). The Figs. 10 and 11 were obtained for two different spectra compositions consisting different amount of protons and iron nuclei in the primary cosmic ray flux. Again as it was expected, the difference of the muon distribution slopes seen is not a big one and can be seen only in those  $(\rho_\mu, \rho_e)$  bins which lay close to the center of the area occupied by the showers were both: showers initiated by the protons and by the iron give the contribution. On the edges the slopes are determined by the proton (upper edge) and iron nuclei (lower edge).

The realistic situation for more complete mass composition is given in Fig. 12.

All the Figs. 8 – 12 were obtained using the shower generator based on the CORSIKA simulation program (Ref. [4]).

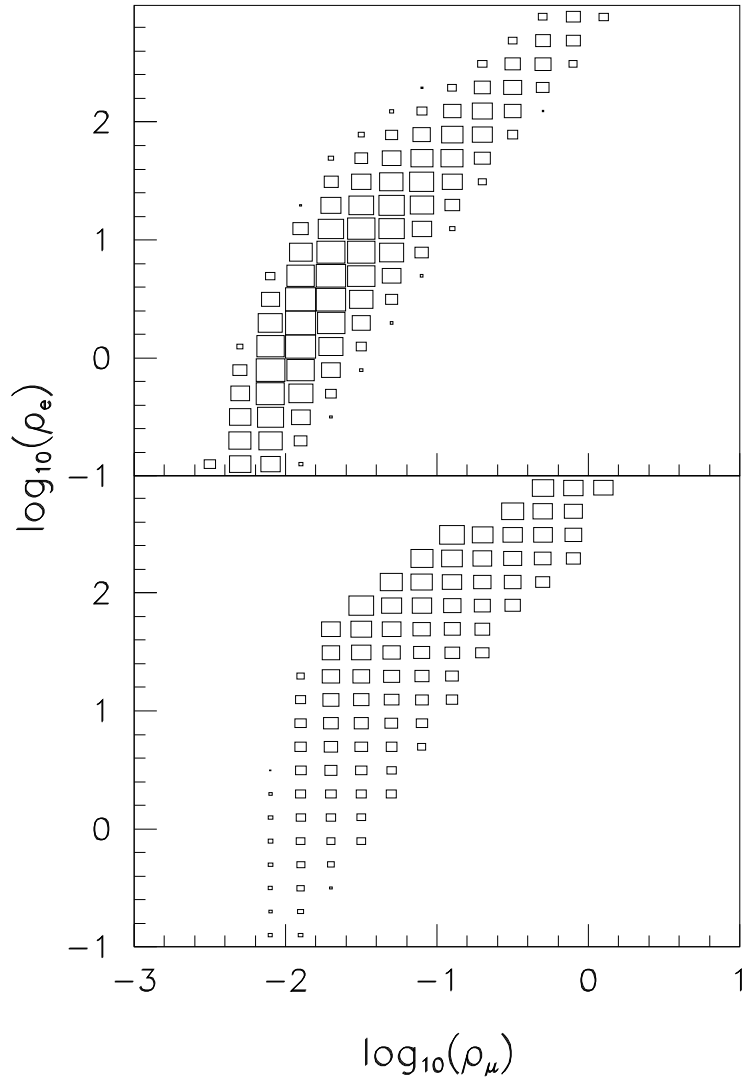


Fig. 8. The results on simulation of pure proton CR primary mass spectrum. The upper figure shows the two dimensional spectrum of  $(\rho_\mu(10m), \rho_e(50m))$ . The size of each boxes is proportional to the logarithm of the number of showers with the given electron density at radial distance 10m and the muon density at 50m. The lower figure presents the slope of the muon distribution at radial distance 50m for each given  $(\rho_\mu(10m), \rho_e(50m))$  shower subsample. The size of each box is proportional to  $-\left(\frac{d \ln \rho_\mu}{d \ln r}\right)$ .



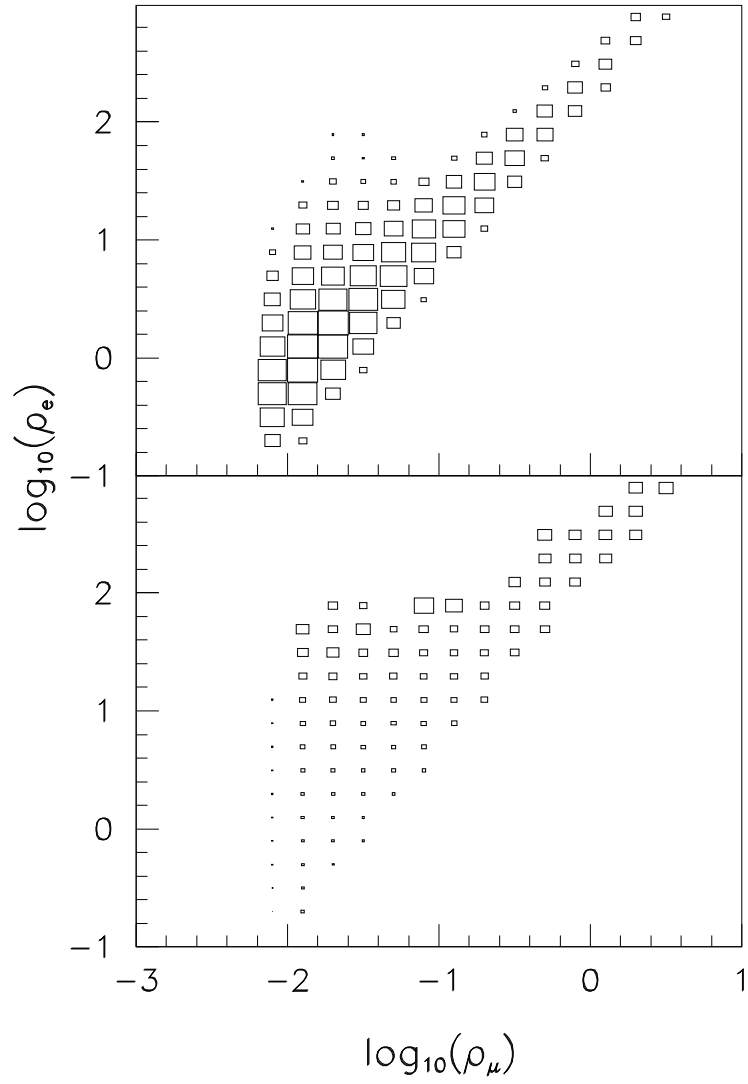


Fig. 9. The results on simulation of pure iron CR primary mass spectrum. Description as for Fig. 8.

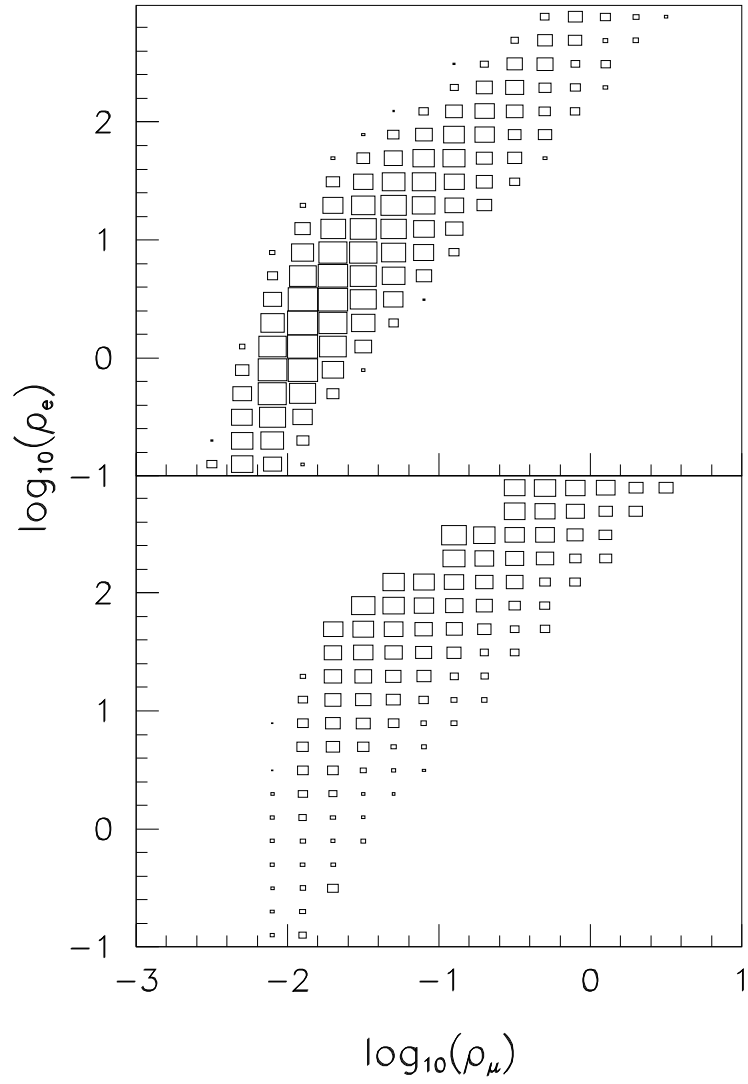


Fig. 10. The results on simulation of 80% iron and 20% of protons in the CR primary mass spectrum. Description as for Fig. 8.

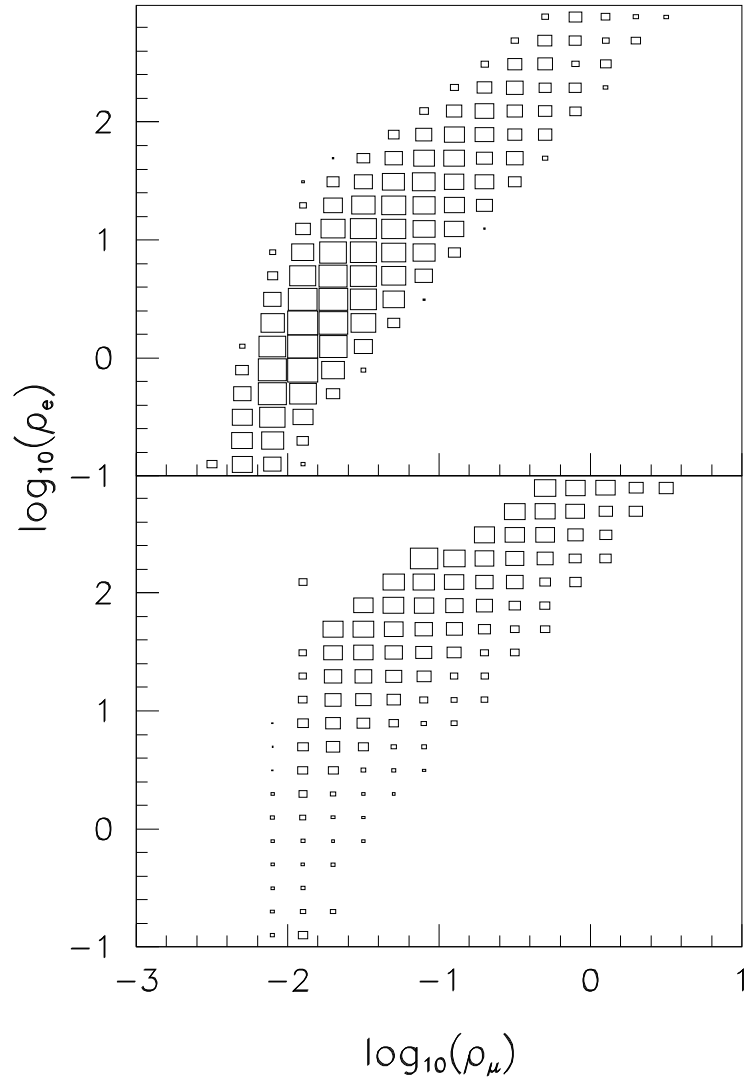


Fig. 11. The results on simulation of 60% iron and 40% of protons in the CR primary mass spectrum. Description as for Fig. 8.

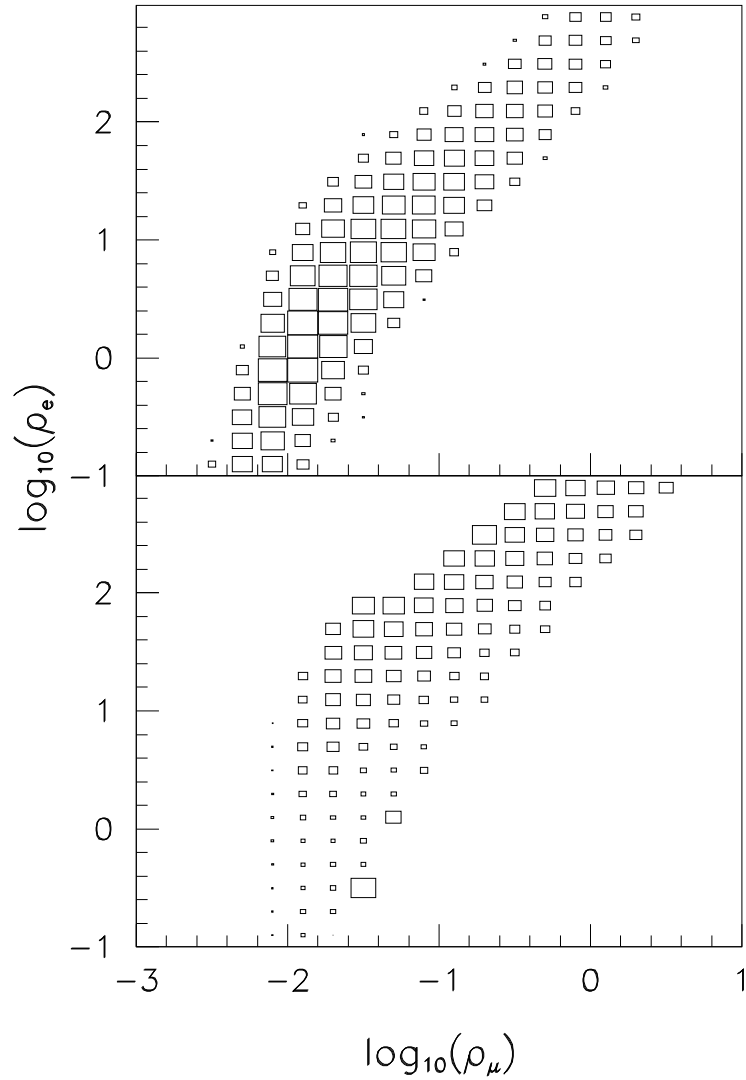


Fig. 12. The results on simulation of JACEE CR primary mass spectrum. Description as for Fig. 8.

### 3 Summary

Fig. 12 shows that the few weeks of the operation of the the KASCADE experiment will be enough to proof the ability of the CR mass spectrum determination with the method of the individual Extensive Air Shower study.

The proposed method of the data analysis is free of any Monte-Carlo simula-

tion based predictions and arguments. (It can be called "model independent".) Of course if one wants to obtain a detail information about the primary mass composition ( in principle from the plots like that in the Fig.7 it is possible ) he ought to assume at least the  $\mu$ -slope as a function of  $\rho_\mu$  and  $\rho_e$  for proton showers and the  $(\rho_\mu(r_0), \rho_e(r_0))$  proton shower spectrum (as that like in upper part of the Fig.8) but it is "simulation dependent", to some extend of course.

The analysis also will give the proof of the usefulness of the  $\mu$ -slope parameter for the multiparameter individual shower study of the primary CR mass composition in KASCADE experiment.

#### 4 Appendix: Accuracy of shower parameters determination

The results presented above in Figs. 8 – 12 were obtained only using the shower generation algorithm without taking into account the real apparatus performance. The important question is if the uncertainties due to the shower reconstruction procedure for a given particular EAS array do not introduce too much distortion to the data interpretation. That question can be answered only by testing the data evaluation procedures. For the KASCADE array geometry the quality of the data collected by the large amount of detectors distributed over the  $200\text{m} \times 200\text{m}$  area is expected to be good enough for a discussed above purposes specially for the bigger showers. In the Fig. 13 there are given the accuracies of shower parameter determination important for the purposes discussed above.

It can be seen that for small showers (primary energy of about  $10^{16}\text{eV}$ ) the accuracy of the muon slope parameter defined as

$$\alpha(r_0) = - \left. \frac{d \ln \rho_\mu}{d \ln r} \right|_{r=r_0} \quad (1)$$

is rather poor. But the  $10^{17}\text{eV}$  showers are big enough to be used directly as it was proposed. However for the small showers the situation is not hopeless. The muon distributions for each  $(\rho_e, \rho_\mu)$  bin can be averaged for many showers and after that the slope determination can be performed.

In the Figs. 14 and 15 there are 3-dim plots like that in Figs. 8 – 12 for the showers used for the quality test in the Fig. 13. Upper figures shows again the number of showers in each  $(\rho_e(50), \rho_\mu(50))$  bin (the size of the box is proportional to the logarithm of the number of hits) and the lower shows the average slope in each bin (here the size of the box is proportional to the  $\alpha(50\text{m})$ ). The plots in the Fig. 14 shows the *true* shower values while the results obtained by the evaluation of the detected particle numbers *reconstructed*

*events* are given in the Fig. 15. As it can be seen for the  $10^{17}eV$  showers the change of the muon slope seen in generated events is still seen in reconstructed events.

The mass composition assumed here is the JACEE one, for all the Figs. 13 – 15. It should be noticed that for both energies only 10000 showers were used to make that figures.

For the shower reconstruction there was assumed that the detector are "ideal". This means that the detector response width was set to 0. The fluctuations of the detector response are due only to the extensive air shower development physics.

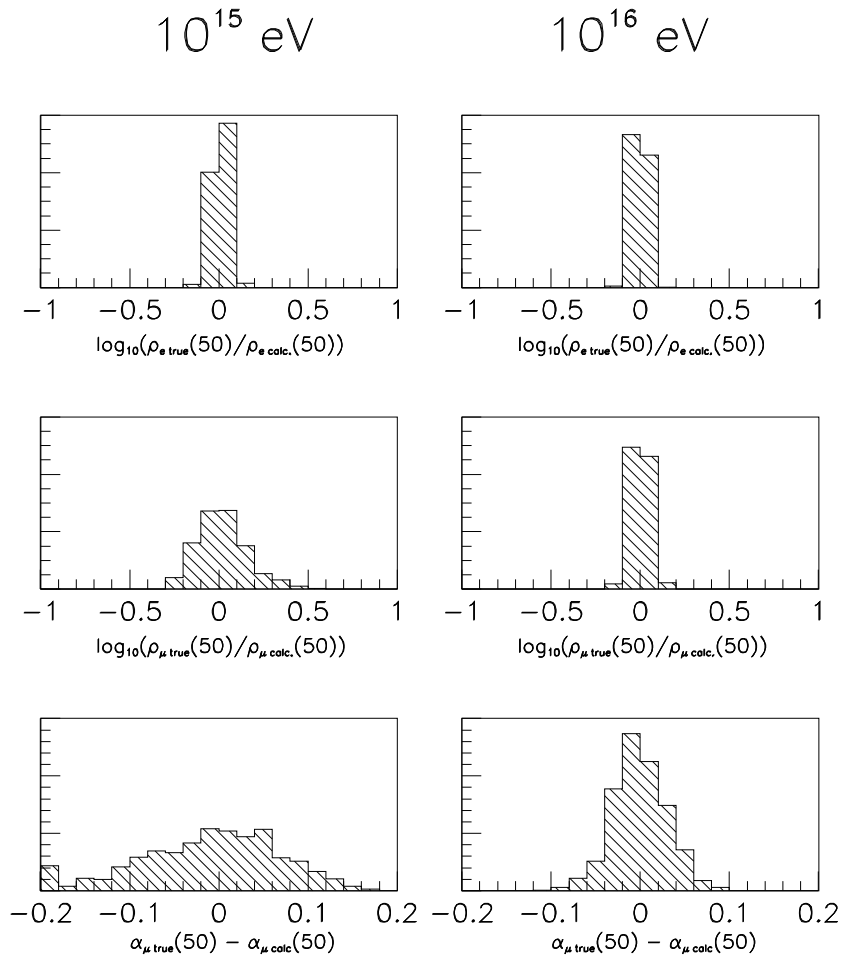


Fig.14. The errors in the shower parameters determination. The primary particle energy is  $10^{16}$  eV and  $10^{17}$  eV respectively.

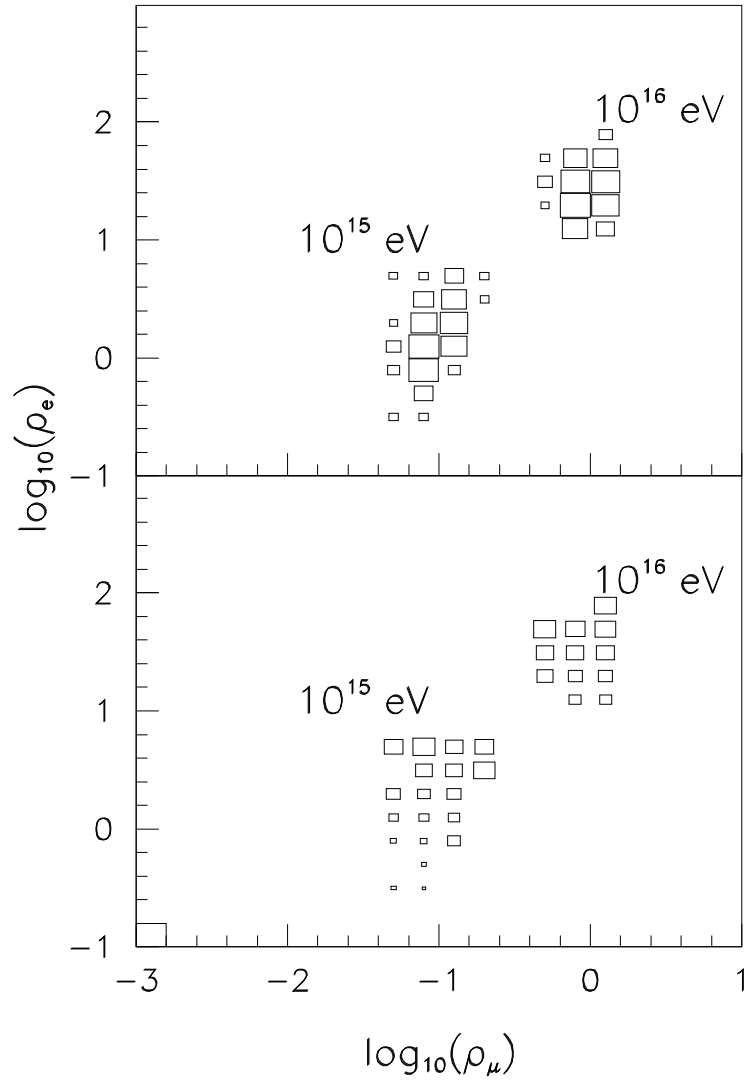


Fig. 15. The spectrum of  $(\rho_\mu(10m), \rho_e(50m))$ . and the slope of the muon distribution as it is given in Fig. 8 for the showers used in Fig. 14.



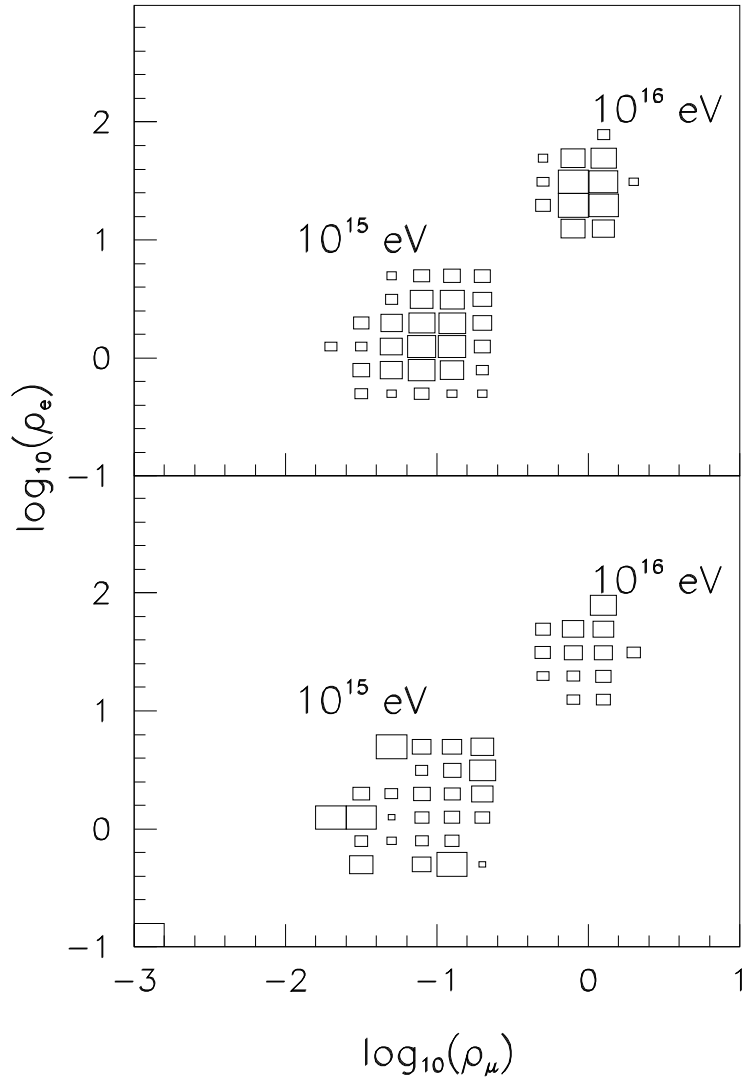


Fig. 16. The spectrum of reconstructed  $(\rho_\mu(10m), \rho_e(50m))$ . and reconstructed slope of the muon distribution as it is given in Fig. 8 for the same showers as used in Fig. 15

## 5 Acknowledgements

I would like to thank Prof. H. Rebel for his useful suggestions and comments.

## References

- [1] H. Rebel and KASCADE collaboration, 7<sup>th</sup> ISVHCRI Ann Arbor, AIP Conference Proc. ed. L. Jones, 575, (1992); G. Schatz, Interdisc. Sci. Rev. **18**, 306 (1993).
- [2] G. Schatz, T Thouw, K. Werner, J. Oerschlaeger and K. Beck, J. Phys. G **20**, 1267 (1994).
- [3] K. Asakimori et al., Proc. 24<sup>th</sup> ICRC Roma **2**, 707 (1995).
- [4] J. N. Capdevielle et al., KfK Report 4998 (1992); J. Knapp and D. Heck, *CORSIKA User's Manual*, Internal Report Forschungszentrum Karlsruhe 1995 (unpublished).